Astron. Astrophys. 230, 21–36 (1990)

ASTRONOMY AND ASTROPHYSICS

IRAS sources beyond the solar circle

II. Distribution in the galactic warp ⋆

J. G. A. Wouterloot [1,⋆⋆], J. Brand [1,⋆⋆⋆], W. B. Burton [2], and K. K. Kwee [2]

[1] Max-Planck-Institut für Radioastronomie, Auf dem Hügel 69, D-5300 Bonn, Federal Republic of Germany
[2] Sterrewacht Leiden, P.O. Box 9513, NL-2300 RA Leiden, The Netherlands

Received April 12, accepted August 3, 1989

Abstract. The distribution of molecular clouds in the outer Galaxy is derived and compared with that of the H I gas layer. Candidate clouds were selected (as described in Paper I) from the IRAS Point Source Catalog on the basis of location on the sky in the second and third galactic quadrants and on the basis of infrared radiation characteristics consistent with those known to be typical of molecular clouds with embedded heat sources. Of the 1302 selected IRAS sources, 1077 revealed CO $J=1-0$ emission and subsequently provided a kinematic distance. Both the number of outer-Galaxy clouds and the range of distances are larger in the sample investigated here than in what has previously been available. The completeness of the sample is discussed, as is the nature of possible errors in the distance determinations, which are based on the almost-flat rotation curve $\Theta=\Theta_0 . (R/R_\odot)^{0.0382}$ derived by Brand and collaborators evaluated for the galactic constants $R_0=8.5$ kpc and $\Theta_0=220\,\mathrm{km\,s^{-1}}$. The molecular clouds in the sample can be traced to about 20 kpc from the galactic center. Because the clouds detected all have embedded IRAS sources, the results here suggest that star formation is occurring in the far outer Galaxy. The ensemble of clouds shows the same warped shape and flaring thickness as shown by the outer-Galaxy H I gas layer. The warp can be followed in the IRAS-selected molecular clouds from its onset near $R=11$ kpc to the edge of the ensemble near 20 kpc. Over this range, the z-thickness of the ensemble increases smoothly, approximately doubling between 10 and 17 kpc. Although the H I layer is substantially thicker than the molecular one in the inner Galaxy, the two tracers approach the same thickness in the outer Galaxy. Comparison of the radial scalelengths of the H I and molecular clouds determined at $R>14$ kpc shows that the H I gas layer terminates less abruptly than the cloud ensemble.

Key words: interstellar medium: kinematics and dynamics of – galaxy: disk of – galaxy: kinematics and dynamics – infrared sources: IRAS.

Send offprint requests to: J.G.A. Wouterloot

⋆ Partly based on observations made at the European Southern Observatory, La Silla, Chile

⋆⋆ Present address: I. Physikalisches Institut, Universität zu Köln, Zülpicher Strasse 77, D-5000 Köln 41, Federal Republic of Germany
⋆⋆⋆ Present address: Osservatorio Astrofisico di Arcetri, Largo Enrico Fermi 5, I-50125 Firenze, Italy

1. Introduction

The early Dutch and Australian 21-cm surveys of the Galaxy revealed that the layer of atomic hydrogen in the outer parts of the Milky Way is systematically warped away from flatness (Burke, 1957; Kerr, 1957; Oort et al., 1958). Although the knowledge of the shape of the outer-Galaxy H I layer has been improved and extended in important ways, the early description remains unchanged in its essentials: the H I layer is severely warped to positive z heights in the northern data, and to negative ones in the southern; furthermore, the H I layer flares, becoming thicker at larger distances from the galactic center (cf. Henderson et al., 1982; Kulkarni et al., 1982; Burton and te Lintel Hekkert, 1986).

Interest in the Milky Way warp increased as it became clear that large-scale, systematic deviations from a flat disk are a common aspect of the H I morphology in the outer regions of spiral galaxies. Many favorably viewed (i.e. edge on) spiral galaxies show an integral-sign shape in the projected H I density characteristic of a warp (see e.g. Sancisi, 1983). Other spirals, less favorably viewed, nevertheless reveal a warped outer shape on the basis of twists in the 21-cm velocity of their line of nodes (see e.g. Bosma, 1981). The hydrogen layers of the nearest large spirals, M 31 and M 33, are both warped: the flaring H I warp in M 31 resembles that in the Milky Way (Brinks and Burton, 1984); the warp in M 33 is a more severe one (Rogstad et al., 1976). Although our embedded perspective of the Milky Way complicates many investigations of galactic structure, it is an ideal perspective from which to study the warped gas layer.

Enhanced motivation for the study of the shape of the outer reaches of galaxies has been provided by the realization that the unobserved dark matter dominating their gravitational potential can be traced most effectively by studying the shape and motions of whatever tracers are accessible at large distances from their centers. Essentially all of the detailed information on the shape and motions of the outermost parts of spiral galaxies, including of course our own Milky Way, has been provided by observations of the 21-cm line of H I. For a variety of reasons, it is important to extend knowledge of the outer Galaxy beyond what is provided by the 21-cm data; the problem of identifying tracers other than H I in the outer Galaxy is made complicated, however, by the fact that all of the other galactic tracers accessible on a transgalactic scale show a morphological confinement to the inner Galaxy (see e.g. Burton, 1976). Evidently, the physical circumstances in the outer

Galaxy differ from those in the inner. We note, in particular, that metallicity decreases with increasing R (e.g. Shaver et al., 1983). A specific problem of wide current interest concerns the weakness of the diffuse galactic 100-micron infrared emissivity from $R > R_0$: is this relative weakness due primarily to a paucity of dust compared to the situation at $R < R_0$, to dust of a different characteristic size distribution, or to the weakness of the interstellar radiation field (see e.g. Deul, 1988)?

The low optical surface brightness of our Galaxy at very large R has made it difficult to establish if there is a stellar counterpart to the gas-layer warp. Miyamoto et al. (1988) present some evidence derived from the kinematics of O and B stars that these stars follow the warp to the limit of the data near $R = 10.5$ kpc. A dozen or so optically visible H II regions have been identified at galactocentric distances about twice the solar distance, R_0. Identification of such regions is crucial to determining the rotation law, and thus kinematic distances, at large R (see e.g. Jackson et al., 1979; Blitz et al., 1982; Brand, 1986; Fich et al., 1989). Although the optically identified H II regions have not been found in sufficient number to reveal their outer-Galaxy spatial morphology in great detail, the work of Fich and Blitz (1984) and of Brand (1986) does show that these regions partake in the warp described by the H I data.

Molecular clouds are much more sparsely distributed in the outer Galaxy than in the inner. Substantial observational work in the CO lines has been directed towards mapping the distribution of molecular clouds at $R > R_0$, but the commonly low intensities of the emission, the paucity of clouds, and the enormity of the sky when sampled with small beams, have so far constrained surveys based on a general, uniform grid either to specific regions of small angular extent, observed in detail, or to larger regions, observed at a higher threshold of intensity (see the summary by Dame et al., 1987; see Mead, 1988, and references there). May et al. (1985, 1988) detected some 30 CO clouds in the third quadrant of the Galaxy distributed in a pattern extending up to galactocentric distances (calculated, as are all distances quoted in the present paper, on a scale corresponding to $R_0 = 8.5$ kpc) of about 13 kpc and inclined with respect to the galactic equator. This provided evidence that molecular clouds without optically identified H II regions (cf. Fich and Blitz, 1984) also follow the galactic warp. The same conclusion was obtained by Mead (1988, and references there), who observed several dozen clouds, located mainly in the first quadrant and clustered near $R = 13$ kpc.

Wouterloot et al. (1988a) showed that IRAS sources can be used as tracers of star formation at galactic radii larger than those which have entered the earlier searches for molecular clouds based solely on CO data. This paper discusses the morphology of the outer Galaxy as revealed by the distribution of some 1000 newly detected molecular clouds at large R. The restrictions of searching for clouds by uniform-grid sampling are avoided by the use of finding charts based on the identification of galactic heat sources that are embedded in molecular clouds and that are listed in the IRAS Point Source Catalog. We selected 1302 outer-Galaxy IRAS point sources and observed them for CO emission as described in Paper I (Wouterloot and Brand, 1989). In this way the molecular cloud ensemble is traced into the distant outer Galaxy, well beyond twice R_0. The cloud distribution shows the same warped shape and flaring thickness that has previously been studied in the H I line. Because the selection procedure provided clouds with embedded infrared sources that are likely to be associated with indications of star formation (e.g. H_2O masers; Wouterloot and Walmsley, 1986), we are also able to conclude that star formation occurs in the far reaches of the Galaxy.

2. Observational material

2.1. CO observations of IRAS sources

Sources were selected from the IRAS Point Source Catalog, Version 2 (1987) according to their position on the sky and according to their radiation characteristics. In order to assure that the selected sources are located in the outer Galactic disk, they have galactic coordinates in one of the following ranges:

(i) $85° < l < 165°$, $-5° < b < 10°$;
(ii) $165° < l < 195°$, $-10° < b < 10°$;
(iii) $195° < l < 280°$, $-10° < b < 5°$.

We argue in Sect. 3 below that the intrinsic distribution of the sources on the sky justifies the skewness in latitude between the ranges selected in galactic quadrants II and III. To identify heat sources of the sort usually associated with regions of current star formation and thus with substantial quantities of molecular gas, we made a further selection based on the following emission characteristics:

(i) The fluxes recorded in the 25, 60, and 100 μm bands are recorded in the Point Source Catalog as detections, not as upper limits.
(ii) The flux at 25 μm is greater than that at 12 μm.
(iii) The ratios R_{ij}, which are the ratios of $\log(\nu S)$ in IRAS band j to that in band i (with bands 1, 2, 3, and 4, corresponding to wavelengths of 12, 25, 60, and 100 μm, respectively) are such that

$$0 < R_{23} < 1.5 \text{ and}$$
$$-1 < R_{34} < (0.261 + 0.227\, R_{23}).$$

These radiation selection criteria discriminate in favor of point sources with infrared emission corresponding to effective color temperatures typical of star-forming regions in molecular clouds that are frequently associated with H_2O maser emission (Wouterloot and Walmsley, 1986) and NH_3 cores (Wouterloot et al., 1988b), while discriminating against those cold IRAS sources which are probably associated with cirrus clumps. Some bright sources that have colors similar to those of T Tauri stars were not selected.

The sample comprises a total of 1302 IRAS point sources, 1292 of which were subsequently searched for CO ($J = 1-0$) emission using the IRAM 30-m and SEST 15-m telescopes and towards the remaining 10 sources we searched for CO ($J = 3-2$) emission using the KOSMA 3-m telescope as described in Paper I. Paper I contains a tabulation of the CO intensity (T_A^*) of each line detected, together with the derived galactocentric and heliocentric distances, the z-distance from the galactic equator defined by $b = 0°$, and the infrared luminosity (L_{IR}). In those cases where the CO spectrum contains more than one line, L_{IR} is given for the component judged to be associated with the IRAS source (in most cases the line with the most extreme velocity).

2.2. H I observations of the warped gas layer

We compare the galactic distribution of the outer-Galaxy molecular clouds identified through their association with IRAS point sources with the distribution of H I gas. The H I data come from the Leiden-Green Bank survey of Burton (1985), from the Parkes survey of Kerr et al. (1986), and from the Berkeley survey of Weaver and Williams (1973). In regions where the surveys

overlap, the Leiden-Green Bank survey was used, principally because of its wide velocity coverage. The composite data cube was further handled following the procedures described by Burton and te Lintel Hekkert (1986). The data cube was transformed from brightness temperatures in an array of heliocentric l, b, v coordinates to H I volume densities (in units of atoms per cm^3) in an array of galactocentric cylindrical coordinates, R, Θ, z. The transformation from v to R was made as described below. The azimuthal angle, Θ, is conventionally measured such that $\Theta = 0°$ for a point infinitely distant in the direction l, $b = 0°$, $0°$ and increasing in the same sense as galactic longitude.

2.3. The velocity-to-distance transformation; potential sources of error

For both the IRAS/CO data and the H I data, we converted velocities to distances using the azimuthally symmetric rotation curve essentially as it was observationally derived by Brand (1986), who combined optical distances to H II regions with velocities from the associated molecular-line emission in the data compiled by Brand et al. (1987). The rotation curve given by the expression

$$\Theta(R) = \Theta_0 \cdot (R/R_0)^{0.0382} \quad (1)$$

with the constants given by $R_0 = 8.5$ kpc and $\Theta_0 = 220$ km s^{-1} (see Kerr and Lynden-Bell, 1986) deviates only slightly from flatness at $R > R_0$, rising slowly to a value of $\Theta = 227.3$ km s^{-1} at $R = 20.0$ kpc.

Some remarks are in order regarding potential sources of error in the derivation of kinematic distances.

Use of a single rotation curve for all galactocentric azimuths depends for its validity on cylindrical kinematic symmetry. It has long been known that the velocity range of H I gas near the galactic equator is systematically larger at fourth-quadrant longitudes than at the complementary first-quadrant ones (see e.g. Fig. 7.10 in Burton, 1988b). The systematic differences in the velocity extents imply large-scale deviations from axial symmetry of either a spatial or kinematic nature. It is not yet clearly established whether the H I distribution in our own Galaxy is *spatially* lopsided in a manner similar to that observed in a number of nearby spiral galaxies, notably M 101 (see Baldwin et al., 1980), or *kinematically* distorted by the galactic potential (Blitz, priv. comm.). The velocity field derived by Brand and collaborators shows that (at least in the azimuth range discussed here) it is at least plausible to explain the global outer-Galaxy asymmetries as spatial asymmetries, because the difference between the smoothed outer-Galaxy rotation curve derived only from data at $l < 180°$ and the one derived only from data at $l > 180°$ is not large enough to account for the difference in the profile extents. Thus the use of a single rotation curve seems justified by observations.

The rotation curve used is a smooth one, which does not take into account irregularities of the sort which might be associated with a localized mass concentration. The work of Brand et al. (1988) showed that the observed outer-Galaxy velocity field has irregularities of up to about 10 km s^{-1} with respect to the azimuthally smoothed velocity curve. Deviations of this amplitude will introduce distance uncertainties of the order of 1 kpc over most of the longitude range discussed here.

We note that local kinematic irregularities will involve local variations in the important kinematic parameter, $|dv/dr|$. Variations in rate of change of velocity along the line of sight could cause the v-to-R relationship to be, in fact, locally multivalued. Some of the clumpiness of emission in the Fig. 3 longitude, velocity diagrams could be due at least partially to line-of-sight velocity crowding rather than entirely to local density enhancements. Our conclusions on the global shape of the outer-Galaxy as traced by the molecular clouds associated with IRAS point sources and by 21-cm emission would not be seriously effected by local variations in $|dv/dr|$ because of the substantial smoothing over ranges in both azimuth and radius greater than the extents characteristic of the observed irregularities in the velocity field.

The parameter $|dv/dr|$ is near zero in a wedge centered on $\Theta = 180°$; the linear width of the wedge becomes greater as R increases. Thus the resolution of the v-to-R transformation is poor near $\Theta = 180°$, and becomes increasingly worse in this direction at larger distances. The data in Figs. 4, 7, and 8 pertaining to azimuths within about 15° of the anticenter direction have been ignored in deriving our general conclusions.

For the molecular component we have also derived distances using a detailed, unsmoothed, velocity field, i.e. retaining non-circular motions (see e.g. p. 161 of Brand, 1986; or Brand et al. 1988). This observed velocity field was derived from optically visible H II regions; this detailed approached is therefore only possible for objects closer than about 6 kpc from the Sun. Because the IRAS-selected molecular-cloud sample extends well beyond this limit, and because distances to the diffuse H I component cannot be derived accurately in this way, we have chosen to analyze all data in a uniform way by calculating distances using the azimuthally-smoothed rotation curve. For the molecular component we discuss below differences resulting from these two approaches.

3. Statistics of the IRAS point-source/molecular-cloud sample

A total of 1302 point sources selected from the IRAS Point Source Catalog were searched for emission in the CO ($J = 1-0$) line; of these, 1977 (83%) revealed a CO line with an intensity above the typical threshold of $T_A^* = 1.0$ K.

The distribution on the plane of the sky of the 1077 sources which were detected in the CO line is shown in Fig. 1(a). The most striking aspect of the distribution is the definite tilt of the distribution with respect to the galactic equator. This is the signature of the warped nature of the outer-Galaxy molecular ensemble, which is the subject of the discussion below.

Figure 1(a) shows that the number of detected sources decreases strongly towards the latitude boundaries of the area in which the search was carried out. This indicates that the area searched was chosen large enough to sample the galactic layer adequately, except for those nearby sources at high $|b|$. We estimate from the measured scale heights that about 30% of the molecular clouds associated with IRAS point sources in the range $8.5 < R < 9.5$ kpc will have been excluded by the latitude constraints; their absence will not effect our general conclusions.

Figure 1(b) shows the distribution on the plane of the sky of all selected IRAS point sources which were not detected in CO emission (225 sources). The smooth distribution of the non-detections in l and, especially, b suggests that these IRAS sources are predominantly extragalactic: the distribution is clustered neither towards the galactic equator, nor toward the tilted distribution of the warped galactic layer. The expected number of background galaxies, estimated by applying the same radiation selection criteria scaled to equivalent areas of the sky in two fields at high galactic latitude ($0^h < \alpha < 4^h$ and $12^h < \alpha < 16^h$;

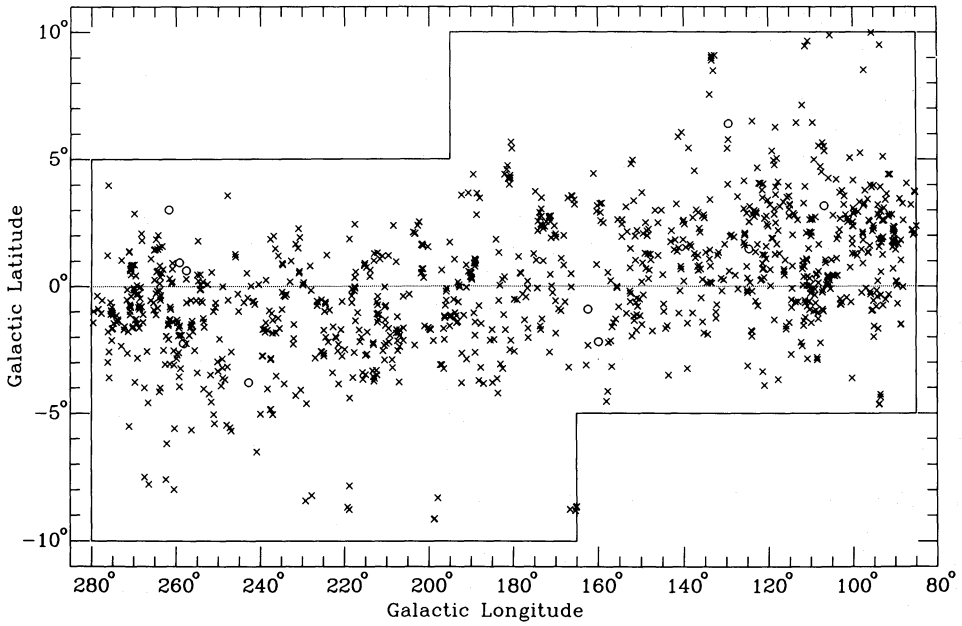

Fig. 1a. Distribution on the plane of the sky of all selected IRAS point sources which were detected in CO ($J=1-0$) emission. Open circles indicate directions of point sources towards which CO was detected but judged not to be associated with the IRAS source. Full-drawn lines mark the positional limits of the region where IRAS point-source catalog was searched for heat sources plausibly associated with outer-Galaxy molecular clouds. The dotted line represents the galactic equator, which is clearly not the plane of symmetry of the detected sources

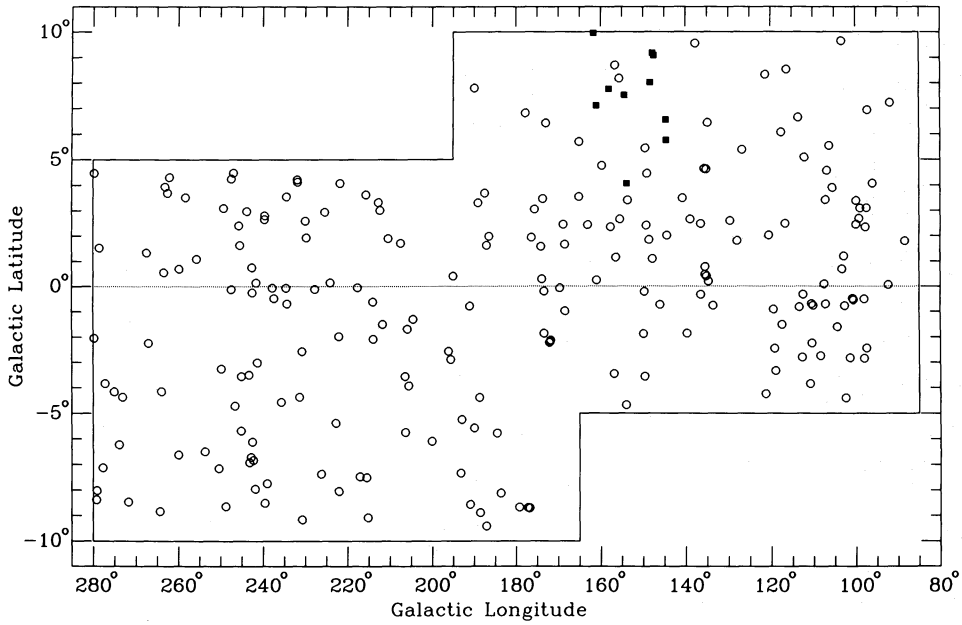

Fig. 1b. Distribution on the plane of the sky of all selected IRAS point sources which were not detected in CO ($J=1-0$) emission (circles) or in CO ($J=3-2$) emission (squares). The lines have the same meanings as in Fig. 1a. The sources which were not detected are probably largely extragalactic

$-10° < \delta < 10°$) is 160 ± 30. In fact, 39 of the IRAS sources which passed our selection criteria are identified as galaxies in the Point Source Catalog. The intense CO emission observed towards some of those sources suggests, however, that these may be infrared sources located within the Milky Way. Another class of sources which is partly included in our sample are planetary nebulae. Twenty two of the selected sources are identified as planetaries in the Point Source Catalog; about half of these were detected in CO, and have lines which are both more intense and narrower than molecular lines characteristic of planetary nebulae, suggesting that at least some of these sources may in fact be compact H II regions.

Some 87 of the sources in the entire sample could be identified with known H II regions; of these, 6 yielded no CO emission above the observational threshold. Two of the 6 may be sources seen projected on very extended H II regions, namely 00187+6127 on S 173 and 05130+3420 on S 229. The remaining 4 sources are located near small H II regions, namely 05075+3755 near S 226, 05247+3422 near S 234, 05281+3412 near S 237, and 07077−1821 near S 301. It is unlikely that these sources are background galaxies because of the strength of the infrared emission (e.g. 05281+3412 emits 932 Jy at 100 microns). They could be bipolar nebulae of the sort typified by 07399−1435 (OH 231.8+4.2), which has comparable IR colors. We conclude that although some of the 1302 IRAS sources in the sample may be galaxies, planetary nebulae, or peculiar objects, the large majority of them are pre-main sequence objects.

The question of the completeness of the sample naturally arises. When investigating the galactic distribution of IRAS sources it is important to include only those sources in our sample

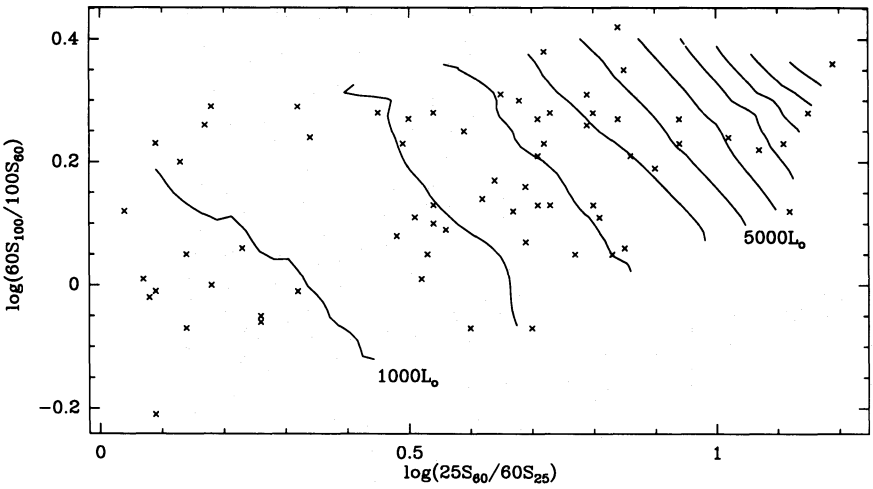

Fig. 2. Limiting luminosity of IRAS sources which would just have been included in the sample if they were at a distance from the Sun of 15 kpc, plotted as a function of 25–60 μm IRAS colors. The contour levels range from 1000 $L_\odot$ to 10000 $L_\odot$ in steps of 1000 $L_\odot$

that would have been detected by the IRAS mission no matter where they were located in the outer Galaxy. This implies limits in luminosity dependent on the colors of the IRAS source. From a comparison of luminosity with heliocentric distance it is seen that no CO is detected more distant than 15 kpc from the Sun. Sources in our sample have *detected* fluxes (not upper limits) at 25, 60, and 100 μm; this, together with the color criteria described in Sect. 2.1, implies that the 25 μm flux alone can be used for a completeness check. In practice this means that $S_{25\,\mu m}$ is larger than 0.25 Jy.

In selecting the complete sample which is used in Sect. 4.3 to derive the distribution of the surface density of IRAS sources in the Galaxy, we checked whether the 25-μm flux of each source, scaled to $r = 15$ kpc, is larger than 0.25 Jy. Figure 2 shows the IR luminosity for sources at this limit, as a function of the 25–60 μm and 60–100 μm colors. The luminosity ranges from about 700 $L_\odot$ for blue sources to about 8000 $L_\odot$ for very red ones. We are thus able to conlcude that the galactic molecular cloud ensemble associated with infrared heat sources more luminous than this limit is completely detected. The absence of IRAS sources more distant from the Sun than 15 kpc is a consequence of the absence of IRAS sources beyond $R = 20$ kpc (see Fig. 4b).

The intrinsic infrared properties of these molecular clouds will be discussed in more detail elsewhere.

4. Kinematic distribution of outer-Galaxy molecular clouds; their distribution projected onto the galactic plane

4.1. Kinematics

Figure 3a shows the arrangement in longitude, velocity coordinates of all CO components detected in the directions of the selected IRAS point sources. It is evident from this figure that a substantial number of molecular clouds has been detected at velocities corresponding to large distances. Figure 3b shows the longitude, velocity distribution of the CO emission components

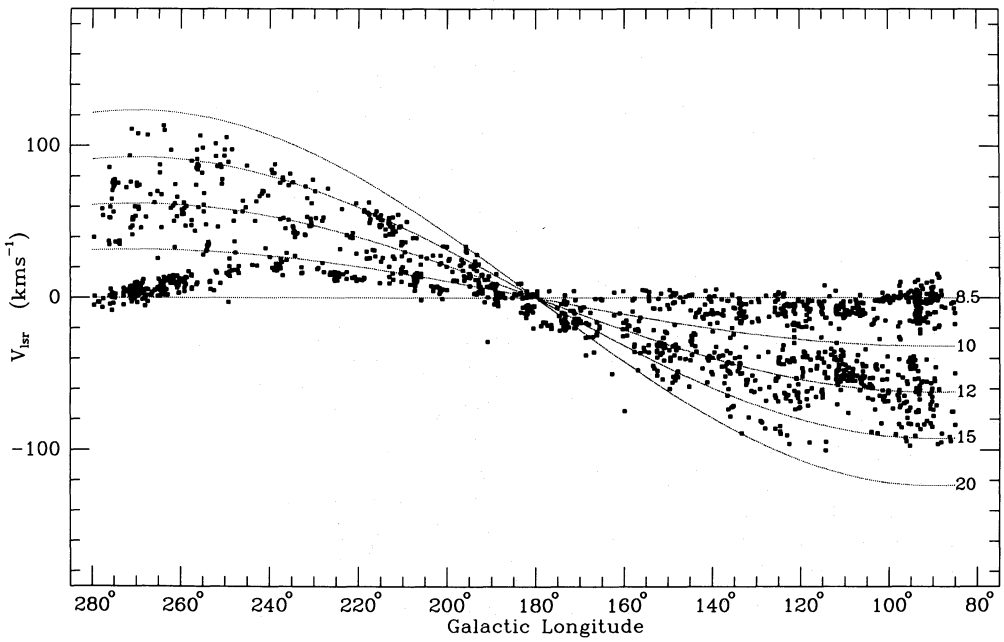

Fig. 3a. Arrangement in longitude, velocity coordinates of all CO emission components detected in the directions of the selected IRAS point sources. The lines show galactocentric circles calculated at $b = 0°$ for the indicated radii using the rotation curve of Eq. (1), with $R_\odot = 8.5$ kpc

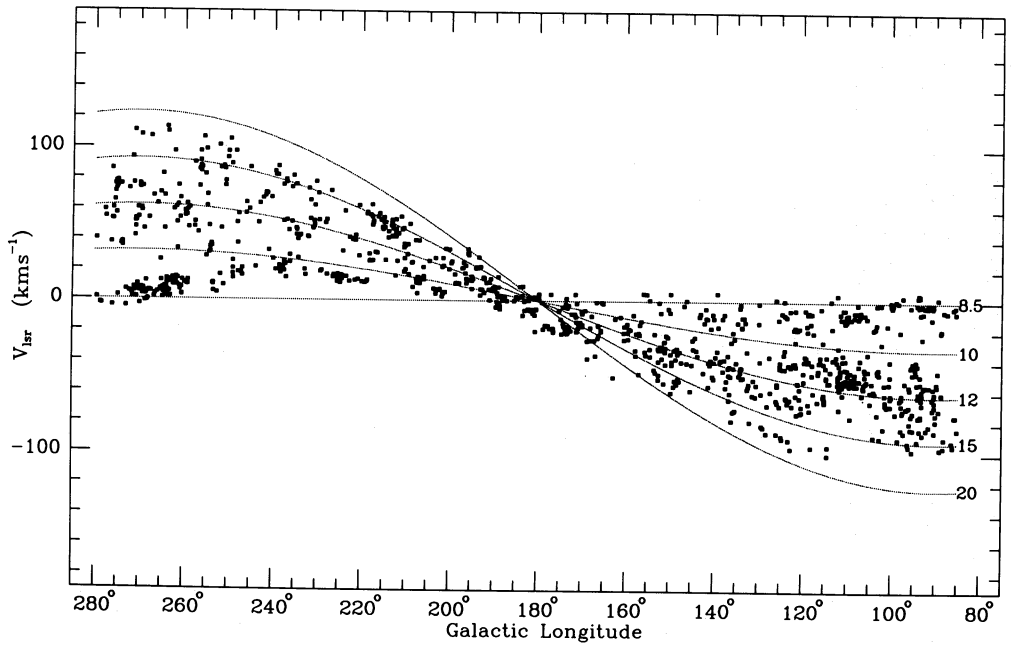

Fig. 3b. Arrangement in longitude, velocity coordinates of the CO emission components which were judged to be physically associated with one of the selected IRAS point sources. The lines indicate constant galactocentric radii. The galactic molecular ensemble is sampled to $R > 2\,R_{\odot}$

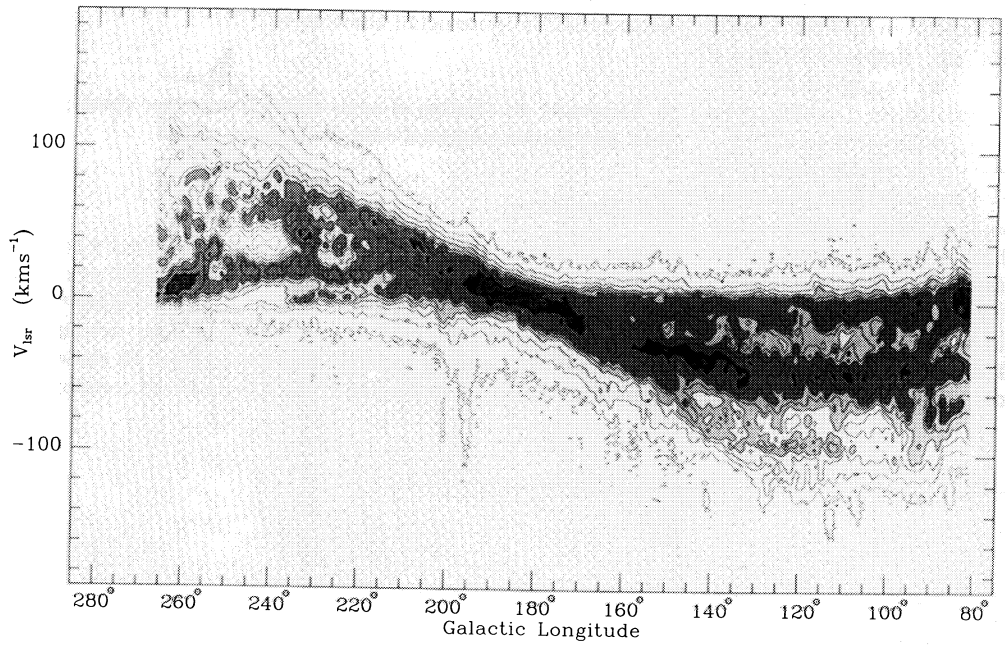

Fig. 3c. Arrangement in longitude, velocity coordinates of H I emission observed along the galactic equator. The 21-cm data are from the Leiden-Green Bank survey of Burton (1985). The lines indicate constant galactocentric radii. Contours are drawn at levels of $T_A = 0.5$, 2, 4, 10, 20, 30, 50, 70, and 90 K. The grey-scale levels change every second contour level

which were judged to be physically associated with one of the selected IRAS point sources. The criteria for establishing this association are discussed in Paper I.

Comparison of the kinematic distribution of the galactic clouds detected according to the IRAS point-source criteria with the kinematic distribution of clouds selected either by optical identification or by uniform-grid CO sampling indicates that the outer Galaxy has been more deeply penetrated by the IRAS point-source criteria then by the earlier work. For example, Blitz et al. (1982) and Brand et al. (1987) measured the velocities of a compilation of optically identified H II regions and reflection nebulae. Comparison of their data with that in Fig. 3b shows that the kinematic distribution of the optically identified tracers agrees well with that revealed by the IRAS heat sources at $|v| \leqq 50\,\mathrm{km\,s^{-1}}$; such comparison is difficult at more extreme velocities because so many fewer optical tracers than IRAS-identified clouds have been identified. For most of the infrared-selected sources at velocities corresponding to $R > 12$ kpc, whatever optical nebulosity might be associated with them would be generally difficult to identify.

The use of finding charts derived from the IRAS Point Source Catalog has resulted in a larger number of CO molecular-cloud detections, spaced over a more extensive range of velocities (up to $|v| = 110\,\mathrm{km\,s^{-1}}$; see Fig. 3), than has been provided by surveys of CO emission from the second and third galactic quadrants which were based on systematic uniform-grid sampling ($|v| < 50$ to $70\,\mathrm{km\,s^{-1}}$; see compilation of Dame et al., 1987). The third quadrant CO survey of May et al. (1985, 1988) of the region $180° < l < 280°$, $-5° < b < 5°$, provied information on some 30 clouds located up to about 9 kpc from the Sun. The May et al.

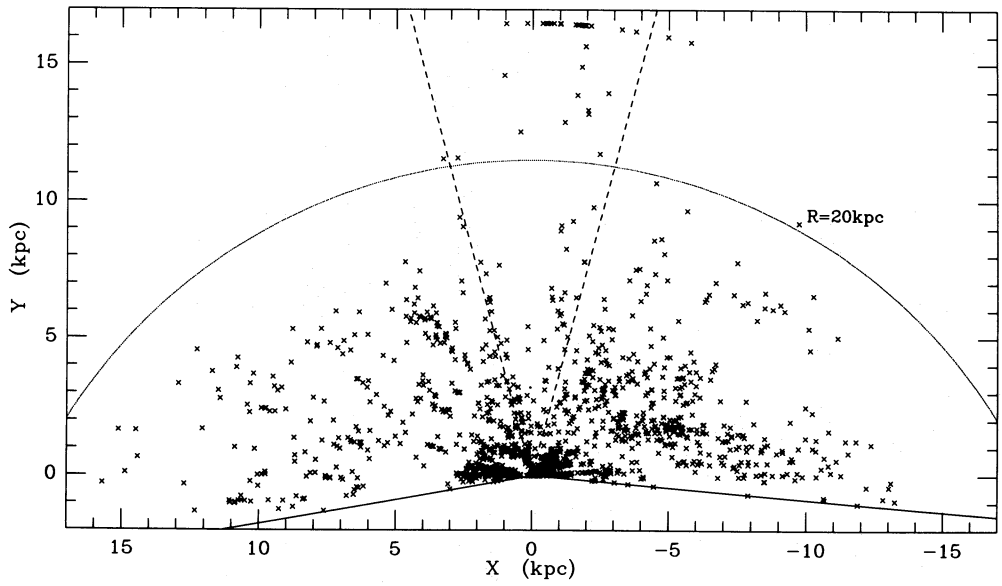

Fig. 4a. Distribution projected onto the galactic plane of all CO emission components detected in the directions of the selected IRAS point sources. The Sun is located at (0, 0); the galactic center, at (0, −8.5). The full-drawn lines show the longitude limits of the point-source sample. The dashed lines mark the region within 15° of the galactic anticenter where kinematic distances are particularly uncertain. The dotted line represents the galactocentric distance $R = 20$ kpc

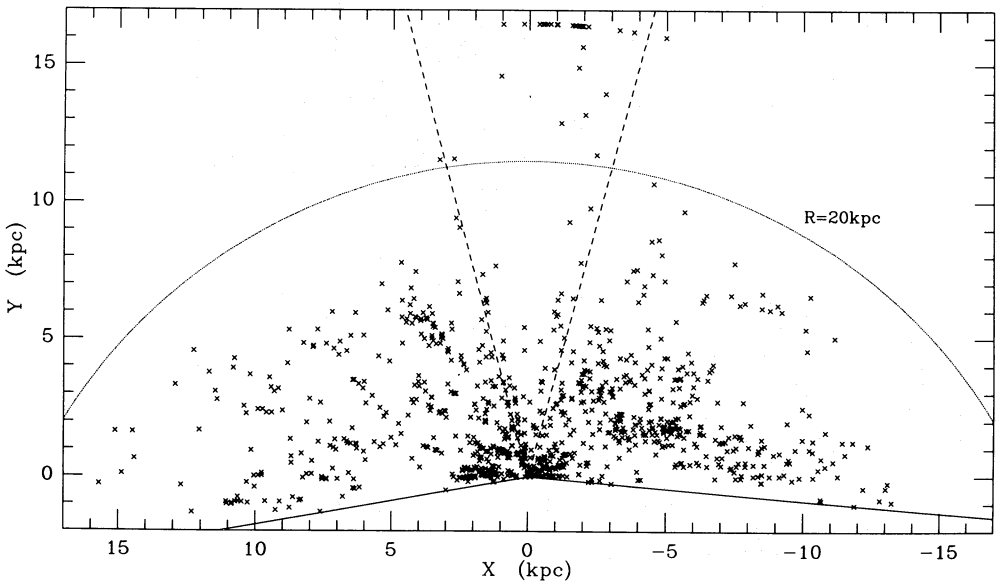

Fig. 4b. As in Fig. 4a, but only for the CO emission components which were judged to be physically associated with one of the selected IRAS point sources

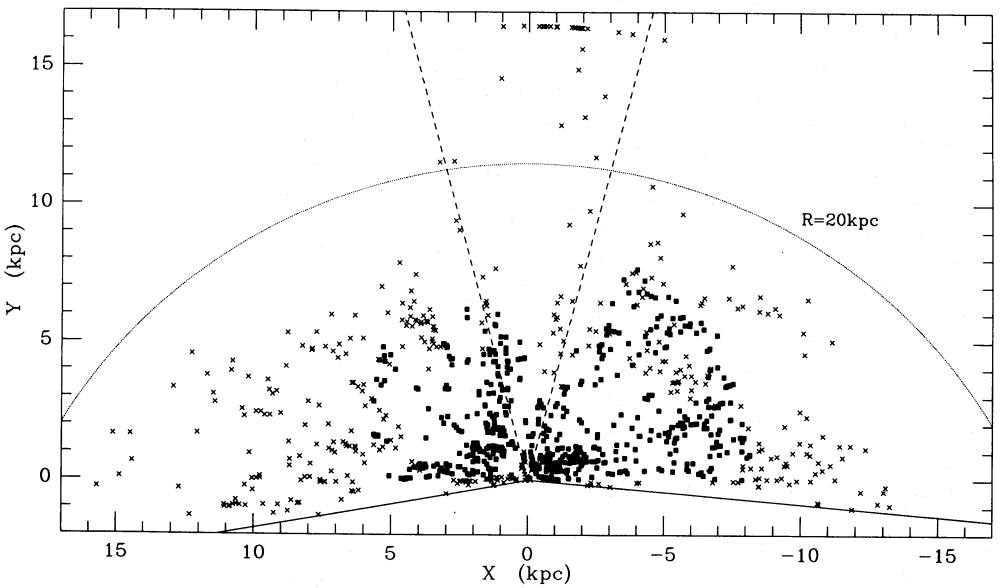

Fig. 4c. As in Fig. 4b, but with crosses representing objects with distances derived from the azimuthally-smoothed rotation curve and with squares representing objects with distances derived from the observed velocity field. In cases the velocity field is multiply-valued with heliocentric distance, the mean distance is plotted

work was carried out with an effective resolution of 0°.5 and a sensitivity threshold of 0.1 K. Maddalena (1986) found, with somewhat higher resolution, a few additional clouds in the region $206° < l < 222°$, $-1° < b < 4°$. Mead (1988 and references there) found 33 clouds clustered near $R = 13$ kpc in the regions $40° < l < 160°$, $-2° < b < 5°$ and $205° < l < 230°$, $-3° < b < 2°$. These CO surveys were made either with a small telescope, involving beam dilution, or with substantial undersampling; the differences between the present results and the earlier ones can be understood in these terms.

Figure 3c shows the longitude, velocity distribution of H I emission along the galactic equator; this can be compared with the distribution of the compact, molecular gas component of the outer Galaxy, as shown in Fig. 3a. In the inner Galaxy the kinematic distribution of the two tracers is quite similar (see e.g. Burton and Gordon, 1978); this seems to be the case also in the outer Galaxy.

The 4 K contour level plotted in Fig. 3c provides a qualitative measure of the kinematic extent of the H I layer which accounts for the intrinsic broadening of the line. The molecular cloud distribution and that of the more diffusely distributed H I have essentially the same kinematic extent. Both distributions show a certain patchiness in l, v coordinates, encompassing scales of several kpc. The emission patches at $|v| < 15$ km s^{-1} have been identified with Gould's Belt and the so-called local arm; patches at intermediate velocities in the region $100° < l < 160°$ are part of the Perseus spiral-arm feature.

4.2. *Spatial distribution*

Figure 4a shows the spatial distribution, projected onto the galactic plane, of all CO emission components detected in the directions of the selected IRAS point sources. Figure 4b shows the spatial distribution of the components which were judged to be physically associated with one of the IRAS heat sources. In cases of multiple features on a single spectrum, the higher $|v|$ feature was usually judged to be associated with the IRAS source; therefore the differences between Figs. 4a and 4b mostly occur for $r < 1$ kpc. Note that 29 sources near $l = 180°$ which were assigned a distance $R = 25$ kpc in Paper I have a relatively large distance uncertainty.

The data plotted in Fig. 4 show that there are few molecular clouds more distant from the galactic center than 20 kpc. Because the strength of the CO lines detected decreases with increasing distance from the Sun but not with increasing galactocentric distance, we may conclude that there is no substantial star formation beyond 20 kpc: evidently, all bright (see Sect. 3) galactic heat sources can be detected by the selection performed here. We note that the Fig. 4 plots do not show the low-extinction "fingers", oriented towards the Sun, which allow optical H II regions to be seen at large distances in certain spatial windows. Distant objects are found in the current data more or less evenly scattered over longitude. The second quadrant is more richly endowed than the third with molecular clouds with embedded heat sources; the second-quadrant clouds are largely concentrated in the region near $R = 12$ kpc (with velocities in the range $-60 < v < -40$ km s^{-1}) and belong to what has been identified as the Perseus spiral arm in studies of optically accessible tracers (cf. Kimeswenger and Weinberger, 1989) and of H I. No large-scale spiral arm feature is discernible in the present data which extends over both the second and third quadrants.

Figure 4c shows the projected distribution of all CO emission components associated with IRAS sources, where the distances for sources closer than 6 kpc from the Sun were derived using the unsmoothed velocity field while those for more distant sources were derived using the azimuthially-smoothed rotation curve. For the nearer-by sources the distances plotted in Fig. 4c can differ by up to two kpc from those plotted in Fig. 4b because of velocity streaming associated with individual structural features, principally the Perseus spiral arm. Use of the unsmoothed velocity field leaves our general morphological conclusions unchanged, although we note that the distance to the Perseus arm is less when the velocity field is used.

4.3. *Surface density*

The variation of surface density with galactocentric distance is shown in Fig. 5. Figure 5a shows the surface density of molecular clouds with embedded IRAS sources. The histograms represent the number per kpc^2 of infrared sources in bins of 1 kpc extent in R, shown separately for the northern-hemisphere range $85° < l < 165°$ and for the southern range $195° < l < 280°$. From information on the vertical thickness of the molecular cloud ensemble, we estimate that about 30% of the sources above the limiting luminosity have been missed in the first bin, $8.5 < R < 9.5$ kpc, because they lie beyond the latitude limits of the sample selected. The data are essentially complete in the bins at larger distances. We note that the number of sources in the northern range is approximately equal (at $R > 13$ kpc, beyond the Perseus-arm regime) to that in the southern range; there is thus little evidence for spatial lopsidedness between the second and third quadrants.

The variation with distance from the center of the Galaxy of the projected H I surface density in units of $M_\odot$ pc^{-2} is shown in Fig. 5b, separately for the two wedges of galactocentric azimuth, $120° < \Theta < 170°$ and $190° < \Theta < 240°$, which correspond approximately to the portions of the Galaxy represented in Fig. 5a.

The variation with R of the number density of optically-identified H II regions is plotted in Fig. 5c for the same longitude and latitude interval as represented in Fig. 5a for the IRAS-selected molecular clouds. The strong local peak for the southern-hemisphere distribution is probably due to contamination by reflection nebulae which, because of the selection criteria, do not enter the northern data.

Figure 5a shows that the ensemble of molecular clouds with embedded infrared sources extends well beyond $2\,R_\odot$, to about $R = 20$ kpc; it has not previously been possible to investigate properties of the Galaxy at such large distances in a tracer other than the 21-cm line. The distribution of molecular sources is rather similar in the northern and southern regions for $R < 10.5$ kpc and for $R > 13.5$ kpc. The clustering of Perseus arm molecular sources between 11 and 13 kpc in the northern range causes the peak in the northern surface density histogram. The surface density of sources decreases smoothly at $R > 13$ kpc; the decrease is much slower than that derived from the earlier, general-sampling surveys of CO, which are relatively incomplete in the outer Galaxy.

Figure 5d shows the surface density of CO clouds with associated IRAS sources derived using the observed velocity field, rather than the smoothed rotation curve. As could already be seen from inspection of Fig. 4c, use of the velocity-field data decreases the amount of structure in the source distribution as a function of R compared to the situation following use of the smoothed rotation curve; in particular, there is not such a pronounced decrease in surface density at $R = 10$ kpc as indicated in Fig. 5a.

Figure 5e shows the radial distributions of the surface densities of H_2 and H I. The plots represent data averaged over the second and third quadrants. The surface density of H_2, $\sigma(H_2)$, was derived by scaling the data in Fig. 5a (after multiplying the IRAS

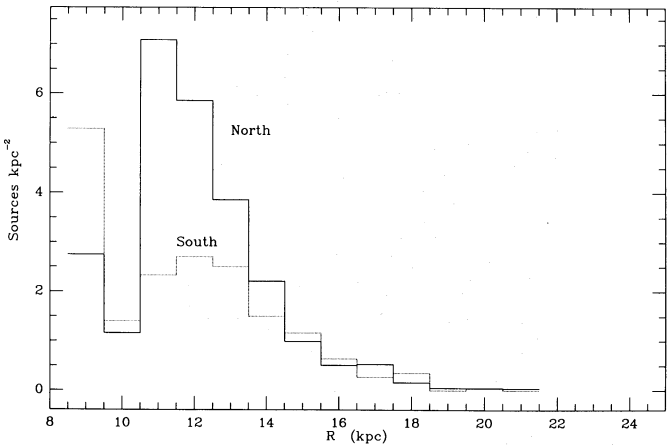

Fig. 5a. Variation with galactocentric distance of the number surface density of the selected IRAS point sources above the relevant L_{IR} as plotted in Fig. 2. The variation is shown separately for the sources in the northern-hemisphere range $85° < l < 165°$ and for those in the southern range $195° < l < 280°$; sources within 15° of the anticenter are not represented here

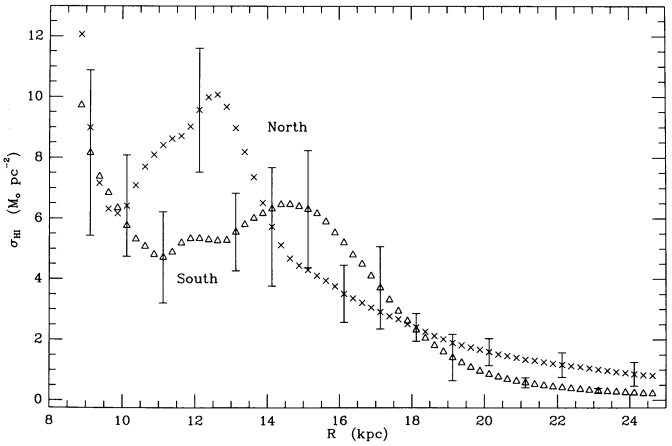

Fig. 5b. Variation with galactocentric distance of the projected H I surface density, in units of $M_\odot$ pc^{-2}. The H I data cube was sampled over galactocentric azimuths $120° < \Theta < 170°$ and $190° < \Theta < 240°$ to reveal H I surface density variations over the portions of the Galaxy comparable to those represented in Fig. 5a for the IRAS-selected molecular clouds

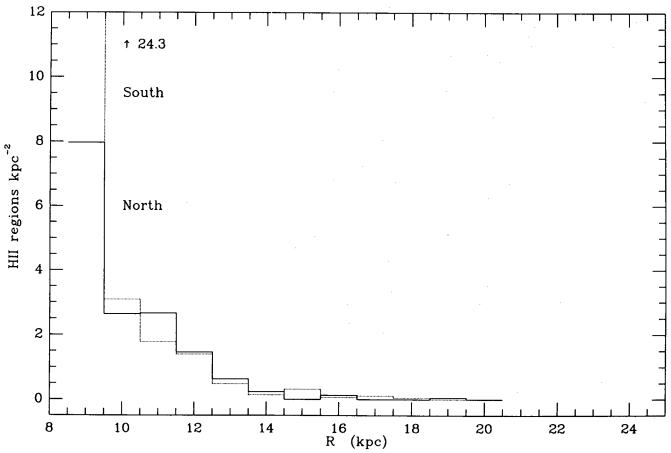

Fig. 5c. Variation with galactocentric distance of the number surface density of optically-identified H II regions plotted separately for the northern data of Fich et al. (1989) and the southern data of Brand (1986)

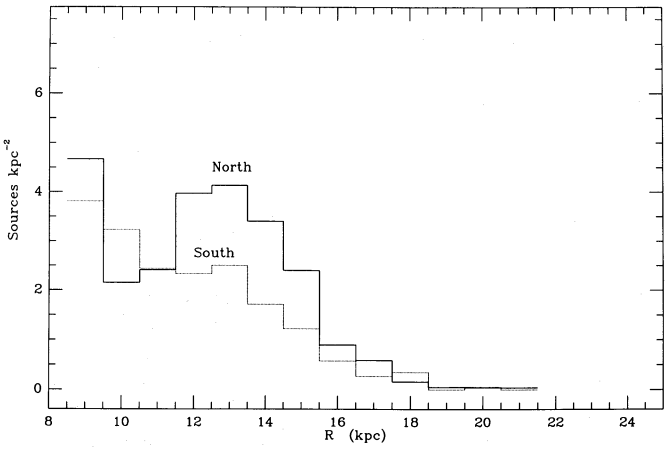

Fig. 5d. As in Fig. 5a, for distances derived from the observed velocity field for clouds in the sample closer to the Sun than about 6 kpc

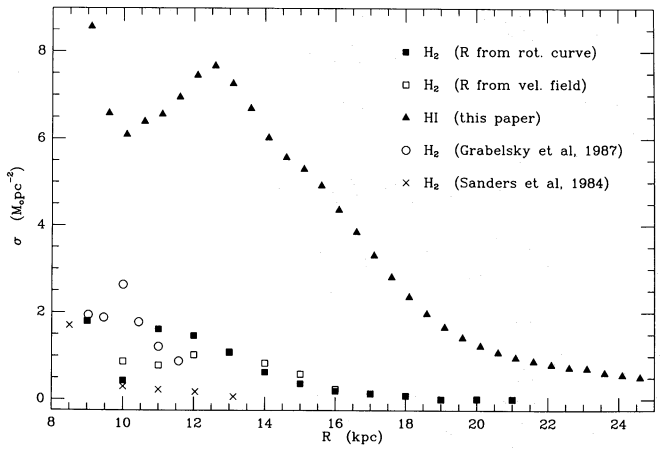

Fig. 5e. Variation with galactocentric distance of the surface densities of H_2 nd H I, averaged over the second and third quadrants. The scaling of the current H_2 data to earlier information pertaining near the Sun is discussed in the text

data for $8.5 < R < 9.5$ kpc by 1.3 to account for the incompleteness due to the latitude limits) with the value of $\sigma(H_2)$ at $R = 8.5$ kpc, $1.8\,M_\odot$ pc^{-2}, derived from earlier CO data. The results of Grabelsky et al. (1987) were used, together with those of Sanders et al. (1984) after converting to the assumptions made by Grabelsky et al. as discussed by Bronfman et al. (1988). Both of the CO data sets were scaled to the values of the galactic constants used here, following the procedures outlined by Grabelsky et al. If one wishes consistency with the scale used by Sanders et al., the H_2 surface densities in Fig. 5 should be multiplied by 2.2. The H_2 surface densities shown in Fig. 5e will in fact be lower limits if the fraction of molecular clouds without star formation is larger at large R than it is in the solar neighborhood. Such could be the case if star formation triggering is independent of the mechanisms which lead to cloud formation.

We note that $\sigma(H_2)$ as derived here decreases more slowly with R than as derived from the earlier, general-sampling CO surveys (cf. e.g. Sanders et al., 1984). Contributing to the more rapid decrease of earlier determinations of $\sigma(H_2)$ is that the observa-

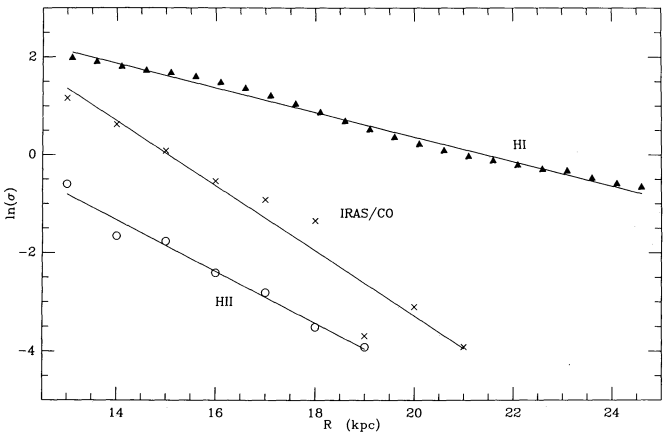

Fig. 6. Rate at which the H I, molecular-cloud, and H II-region surface densities drop off in the outermost parts of the Galaxy shown by the variation with galactocentric distance of the log of the mean surface densities. The means represent the combined data from the second and third quadrants, at $R > 13$ kpc. The surface density decreases approximately proportionally to $e^{(-R/h)}$, where the radial scalelengths for the outer-Galaxy H I, molecular clouds, and H II regions are 4.0, 1.5, and 1.9 kpc, respectively

tional restriction to molecular-cloud data from within a degree or two of the galactic equator will have led to systematic undersampling of the nonplanar, outermost parts of the cloud ensemble.

Beyond $R = 13.5$ kpc, the molecular-cloud surface density distributions are approximately equal in the second and third quadrants. The rate at which the number of clouds bearing IRAS sources drops off in the outermost Galaxy is plotted in Fig. 6. The radial scalelength of the surface density combining the data from both quadrants at $R > 13$ kpc is 1.5 kpc. (Note that the scalelength determined only from data at $R > 13$ kpc will describe only the fall-off of density at the outer edge of the galactic distribution, and should therefore not be compared with scalelengths derived over the entire range of R.) If the relatively poorly-determined distances near $R = 20$ kpc are not included in the determination of the scalelength, the value becomes 2.0 kpc. The scalelength of the surface density of H II regions found at $R > 13$ kpc from the data of Fich et al. (1989) and Brand (1986) is 1.9 kpc.

The H I surface density distribution plotted in Fig. 5b extends beyond $R = 24$ kpc, several kpc further than the molecular cloud distribution. As in the molecular-cloud situation, there is also a peak in the second-quadrant H I distribution at $R = 13$ kpc, corresponding to the Perseus feature. The H I distribution in the third quadrant is approximately flat out to $R = 16$ kpc. At larger R in the part of the Galaxy under consideration here, the southern H I surface density is lower that the northern one. (The well-known spatial or kinematic lopsidedness of the Milky Way is more easily visible when first and fourth quadrant data are compared, rather than second and third quadrant data.) The mean radial scalelength for the second and third quadrant H I surface density at $R > 13$ kpc is 4.0 kpc, as also indicated in Fig. 6. This scalelength is about twice as large as that derived for the outer-Galaxy distribution of IRAS sources.

From our data we derive a total mass of $5.8\ 10^8\ M_\odot$ residing in H_2 clouds at $R > 8.5$ kpc, in good agreement, considering the uncertainties, with that derived by Bloemen et al. (1984) from gamma-ray data. The H_2 mass is an order of magnitude less than the H I mass of $5.3\ 10^9\ M_\odot$ found in the region $8.5 < R < 24.5$ kpc.

In Fig. 5e we also show $\sigma(H_2)$ as derived from the source distribution plotted in Fig. 5d. The run of $\sigma(H_2)$ with R is smoother in this case; the total H_2 mass at $R > 8.5$ kpc is $5.6\ 10^8\ M_\odot$.

5. The warp of the molecular-cloud component of the outer Galaxy; comparison with the shape of the H I layer

It is clear from the current data and from the earlier work cited above that the molecular-cloud ensemble in the outer Galaxy shows the same warped shape and flaring thickness as shown by the H I gas layer.

The different parts of Fig. 7 show the morphology of the H I layer over the range $8.5 < R < 20$ kpc. In this figure maps are plotted in coordinates of galactocentric azimuth and vertical z height showing the distribution of mean hydrogen volume densities in galactocentric cylinders with walls centered at the indicated R. The range of azimuth corresponds to that available for the IRAS/CO sources.

The shape of the outer-Galaxy H I gas layer is revealed by the pattern in the Θ, z variation of densities. At the distance interval closest to the solar distance R_0, the centroid of the H I gas layer deviates from flatness by less than about 200 pc. The systematically warped aspect of the gas layer becomes evident at larger R. The pattern centered at $R = 13$ kpc, shown in Fig. 7c, is approximately sinusoidal; z heights of more than 500 pc above the plane $b = 0°$ are reached in the northern data, and approximately equal deviations below the equator are made in the southern material. The amplitude of the warp traced by the H I layer increases with increasing distance. Thus in the pattern centered at $R = 15$ kpc shown in Fig. 7d, the centroid of the H I layer extends to z heights of about 800 pc near the borders of the azimuth range represented; the centroid of emission centered at $R = 18$ kpc shown in Fig. 7e extends to z heights of more than a kpc.

The global characteristics of the shape of the outer-Galaxy H I layer evident by inspection of the panels of Fig. 7 are consistent with those which follow from the more complete Θ, z information given by Burton and te Lintel Hekkert (1986; see also Burton, 1988a). We note in this regard that the azimuth range of the selected IRAS sources is not large enough to allow accurate measurement of the amplitude of the warp of the molecular cloud ensemble. Investigation of the H I data over the full 360° of azimuth shows that the H I gas layer reaches its maximum height above the plane $z = 0$ kpc at about $\Theta = 80°$, and its maximum distance below that plane at about $\Theta = 260°$. (Figure 7.19 of Burton (1988b) shows for the more detailed H I data the dependence of the warp amplitude on R; Fig. 7.20 from the same reference shows the dependence of the azimuth of maximum excursion from $z = 0$ kpc on R). The azimuthal directions of the maximum H I deviations from the plane do not vary significantly with R. These directions are outside the coverage of the IRAS sample.

The H I gas layer remains quite flat until about 11 kpc from the galactic center. The amplitude of the warp grows linearly, and approximately equally in the two galactic hemispheres, until about $R = 14$ kpc. At larger radii, the amplitude of the warp in the northern 21-cm material continues to increase, until the sensitivity limits of the available 21-cm data are reached at about $R = 23$ pc, where the emission centroid lies at a z height of some 3 kpc. The behaviour of the warp at large distances in the southern-hemisphere material is different: after reaching a maximum excursion of about 1 kpc below the equator at about 15 kpc, the gas layer folds back again towards the equator at the largest distances.

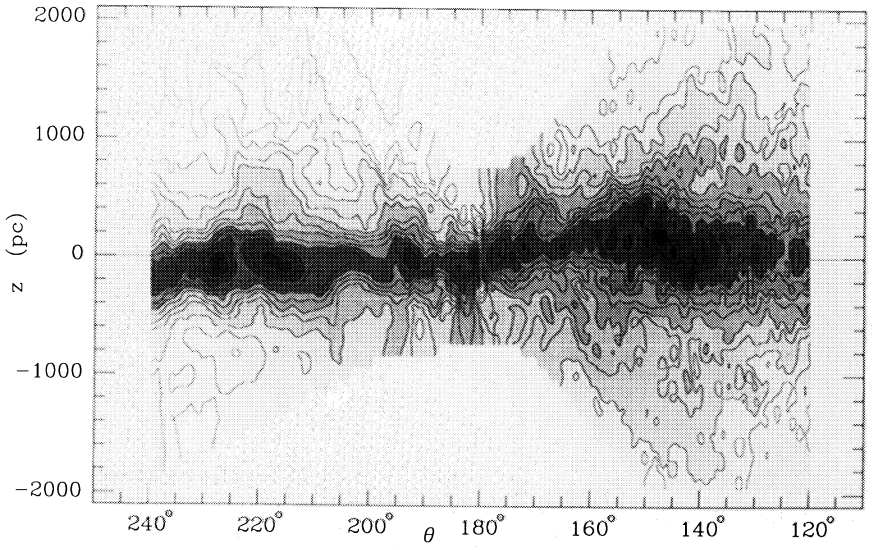

Fig. 7a. Contours of mean H I volume density showing the variation of z height of the gas layer with galactocentric azimuth representative of the region $R = 8.5$ to 10.0 kpc. Contours are drawn at levels of $n_{H\,I} = 0.01$, 0.02, 0.03, 0.04, 0.06, 0.08, 0.12, 0.16, 0.23, 0.31, 0.4, 0.5, 0.65, 0.8, and 1.0 cm^{-3}. The grey-scale levels change every second contour level

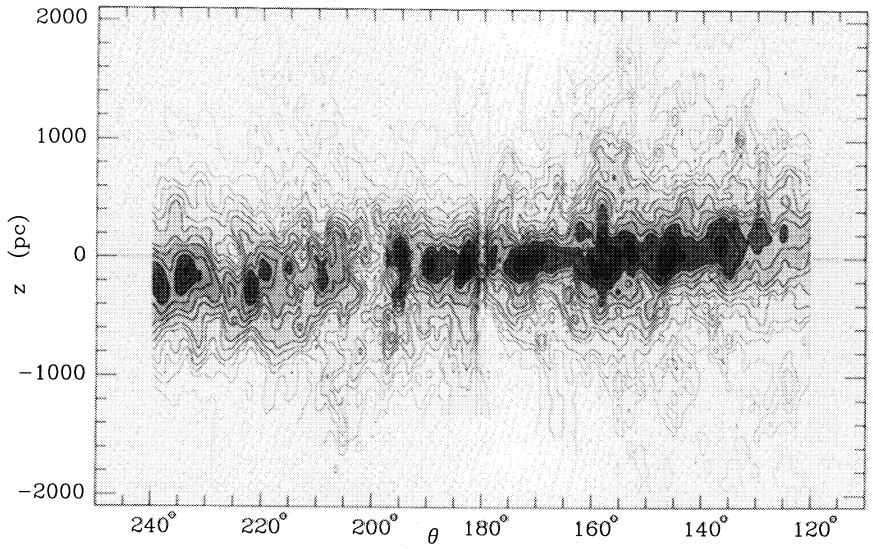

Fig. 7b. Shape of the mean H I gas layer at $10 < R < 12$ kpc

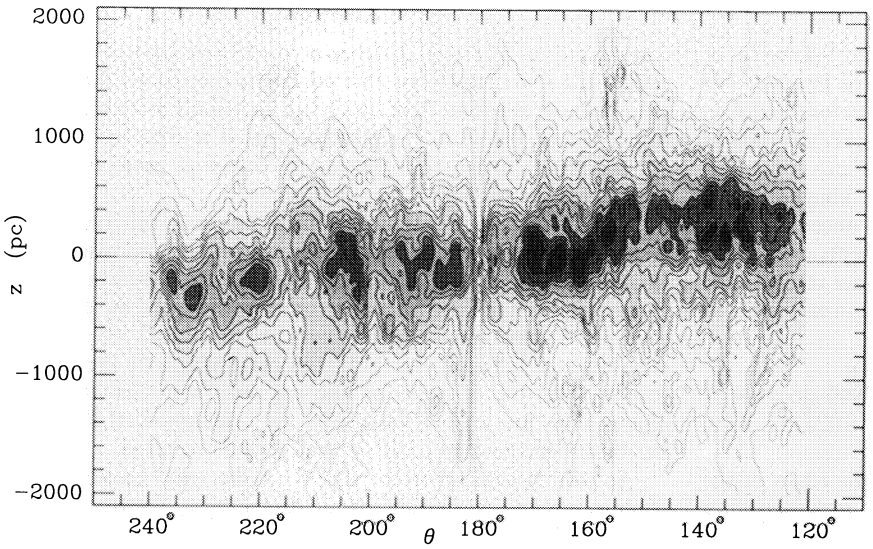

Fig. 7c. Shape of the mean H I gas layer at $12 < R < 14$ kpc

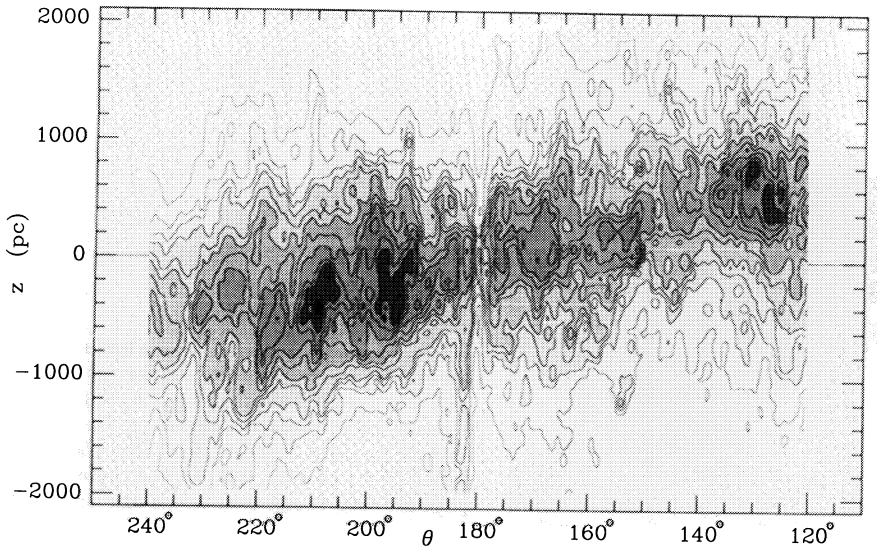

Fig. 7d. Shape of the mean H I gas layer at $14 < R < 16$ kpc

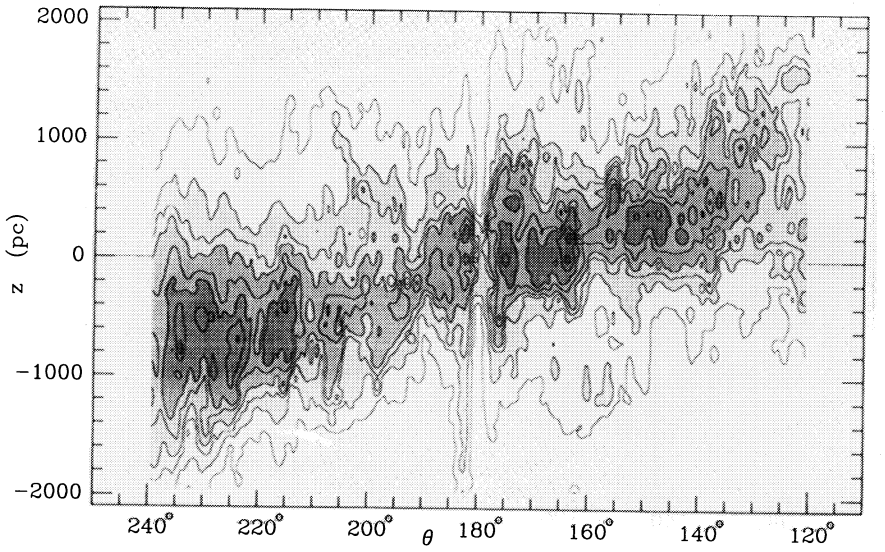

Fig. 7e. Shape of the mean H I gas layer at $16 < R < 20$ kpc

The different parts of Fig. 8 show that the ensemble of molecular clouds partakes in the galactic warp. The figure shows the distribution of z heights as a function of azimuth for the clouds located in the same R intervals as represented for the H I data in Fig. 7. The circles in all panels of Fig. 8 denote clouds located in the anticenter region $165° < l < 195°$ where the kinematic distances, and therefore z heights, are relatively uncertain. The irregular full-drawn line in each panel represents the mean centroid of the H I emission in the indicated distance interval; the dash-dot lines indicate the z height at which the mean emission has fallen to half of its peak value.

The dashed line represents the galactic equator.

Noteworthy sources include IRAS 20505+4940, located at $z = 789$ pc in the second quadrant, and IRAS 07534−3618, located at $z = -956$ in the third.

Also indicated in Fig. 8 are the z-heights at the edges of the distance bins corresponding to the latitude limits of the selection criterion. For example, the 10° latitude limit of the sample corresponds to a vertical distance of more than 1 kpc at the outer edge of the $R = 12$ to 14 kpc interval, and to more than 2 kpc at the outer edge of the 16 to 20 kpc interval. Examination of the source distributions plotted in Fig. 8 indicates that sources at z heights corresponding to latitudes outside the selection range must not occur frequently.

The tilt of the Θ, z pattern of sources increases with increasing distance from the galactic center, indicating in the same way as the H I data that the amplitude of the galactic warp increases with R. Furthermore, the tilted pattern crosses the galactic equator, $z = 0$ pc, at approximately the same azimuth value ($165° \pm 10°$) in each distance interval, for both the molecular and the atomic tracers. The line of nodes of the warped outer Galaxy varies remarkably little with R; evidently the orientation of the warp survives shearing due to differential galactic rotation.

An additional important aspect of the outer-Galaxy morphology is the *flaring* nature of the z distribution. The thickness of the H I gas layer is known to increase steadily from the onset of the

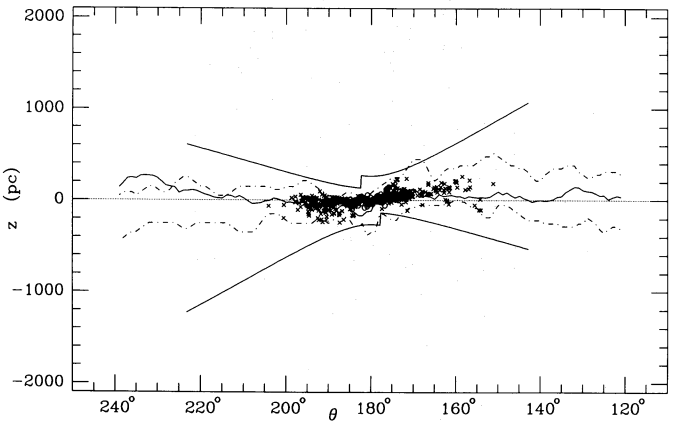

Fig. 8a. Distribution with galactocentric azimuth of the z heights of molecular clouds with kinematic distances in the range $R = 8.5$ to 10.0 kpc

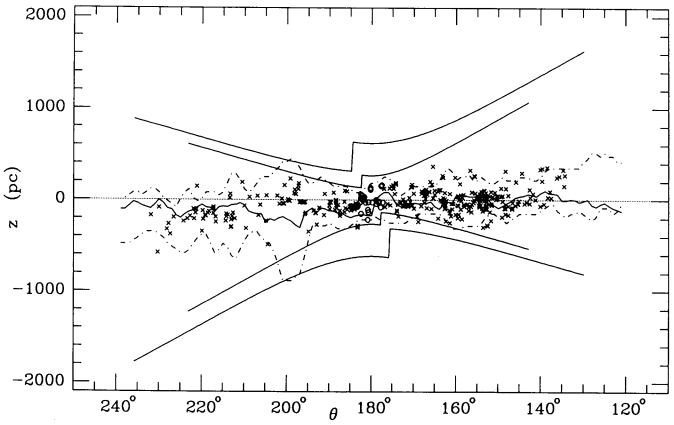

Fig. 8b. Shape of the molecular cloud layer at $10 < R < 12$ kpc

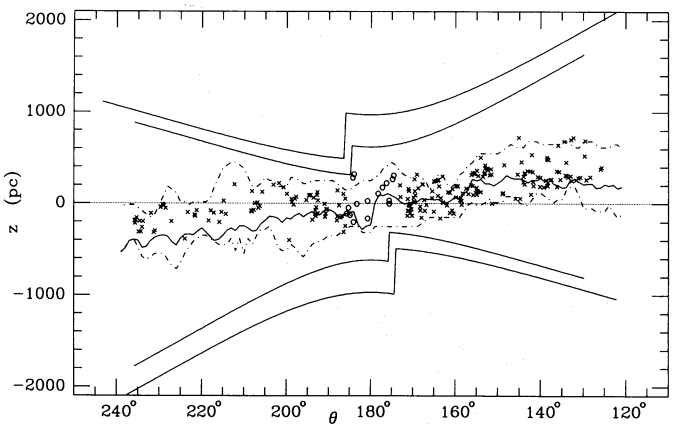

Fig. 8c. Shape of the molecular cloud layer at $12 < R < 14$ kpc

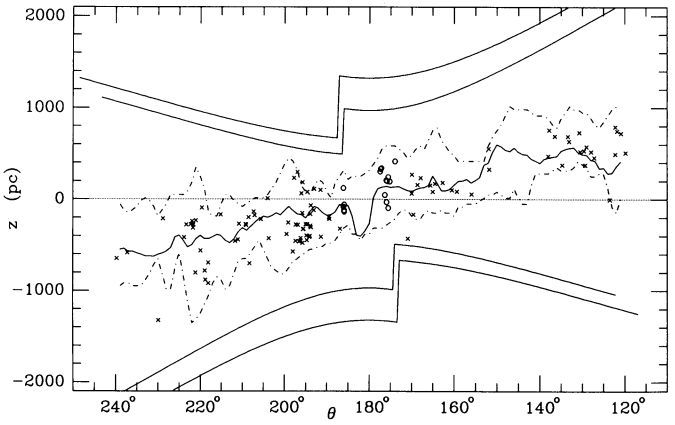

Fig. 8d. Shape of the molecular cloud layer at $14 < R < 16$ kpc

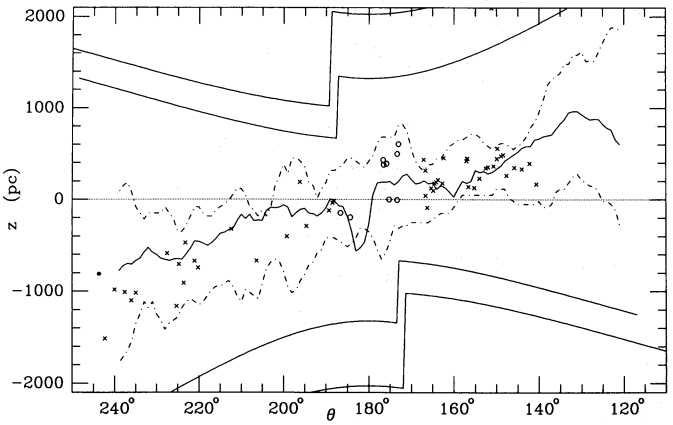

Fig. 8e. Shape of the molecular cloud layer at $16 < R < 20$ kpc

warp, near $R = 11$ kpc, where the thickness of the layer is about 160 pc (measured as the half width at half maximum emission intensity), until the outermost regions where the observational sensitivity limits are reached, and where the thickness is substantially more than a kiloparsec. The Θ, z patterns plotted in Fig. 8 show how the ensemble of molecular clouds with embedded IRAS sources flares in thickness with increasing distance from the galactic center, to distances up to $R = 20$ kpc. The location of the dashed lines in the figure, indicating the thickness of the H I gas layer, shows that the cloud ensemble is contained within the diffuse gas layer.

The above remarks are supported in a more quantiative way by Fig. 9, which compares the thickness of the H I outer-Galaxy gas layer with the thickness of the ensemble of molecular clouds with embedded heat sources. For the H I, the thickness specifies the half width at half maximum of the centroid of the 21-cm emission averaged over bins of 250 pc width in R. For the molecular clouds, the thickness specifies the half width at half maximum of the number distribution of clouds found in bins of 1 kpc width.

Near $R = R_0$, the H I layer measures about 400 pc between half-density points, whereas the ensemble of IRAS-sampled molecular clouds is about half as thick. These measures agree with the solar-vicinity values determined by Lockman (1984) for the principal H I component (as opposed to a thicker layer of warmer, higher-dispersion, but lower-intensity gas), and for the general (i.e. not necessarily containing embedded heat sources) ensemble of molecular clouds as determined e.g. by Sanders et al. (1984). We note in this regard that the layer thickness at R_0 of the widely distributed interstellar dust is approximately equal to the local thickness of the diffuse H I layer but twice that of the molecular layer (Deul, 1988).

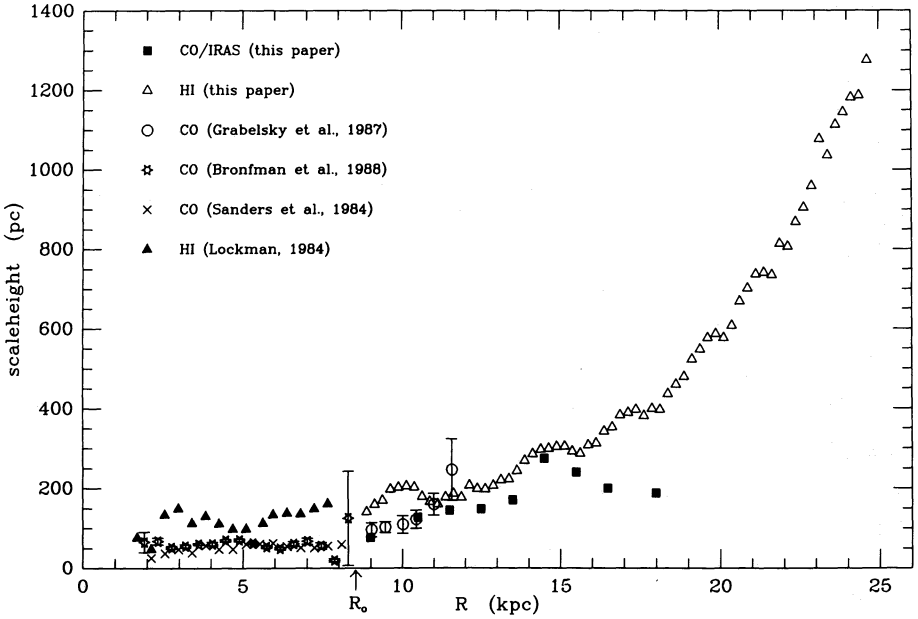

Fig. 9. Variation with R of the thickness of the H I outer-Galaxy gas layer and of the ensemble of molecular clouds. For the H I, the thickness specifies the half width to half maximum of the centroid of the 21-cm emission average over bins of 250 pc width in R. For the molecular clouds, the thickness specifies the half width to half maximum of the number distribution of clouds found in bins of 1 kpc width. The inner-Galaxy results, scaled to $R_\odot = 8.5$ kpc, are included for comparison with the changing situation as R increases

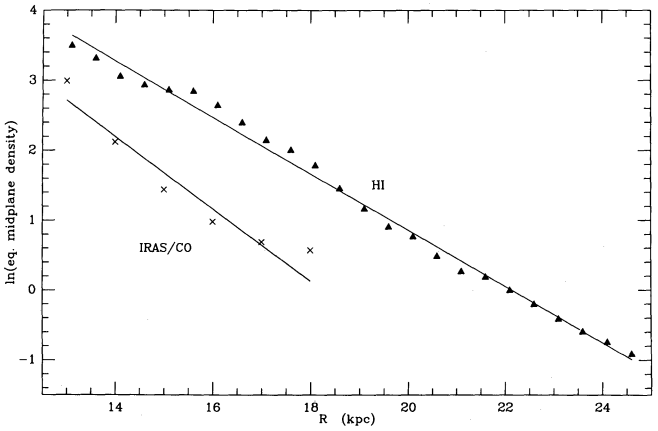

Fig. 10. Variation with R of the equivalent midplane density of the H I gas layer and of the ensemble of molecular clouds with embedded IRAS sources. The radial scalelengths of the H I and molecular-cloud distributions are 2.5 and 1.8 kpc, respectively

At distances greater than R_0, the thickness of both the H I layer and of the molecular-cloud ensemble increase. The increase is small for both tracers until a galactocentric distance of about 10 kpc. At this distance, which we note is the distance at which the warp amplitude also begins to increase more strongly, the thicknesses also increase. At a distance of about 17 kpc the thicknesses of both tracers have approximately doubled compared to the values at 10 kpc. Over the range of distances where the IRAS-selected clouds are available for comparison with the H I data, the molecular thickness is systematically less than the H I thickness, but the relative difference is less than that measured in the vicinity of the Sun. Thus at $R = 15$ kpc, the full H I thickness is 600 pc and the cloud ensemble thickness is 510 pc. The Fig. 9 plot shows that a distances greater than 20 kpc, i.e. beyond the distribution of clouds with evidence of embedded star formation, the diffuse H I layer continues to flare.

For comparison with the situation in the unwarped part of the Galaxy, we include in Fig. 9 the half-thickness values obtained from CO surveys of the inner Galaxy by Sanders et al. (1984) and Bronfman et al. (1988) and of the fourth quadrant out to $R = 11$ kpc by Grabelsky et al. (1988), as well as the H I half thickness in the inner Galaxy determined by Lockman (1984). These data were converted to the $R_0 = 8.5$ kpc scale. For both tracers of the galactic gas layer, the warp as well as the flare of the layer becomes well-defined a kpc or two beyond the solar radius.

The mean volume density of gas in the midplane of the warped gas layer follows from the measures of the layer thickness and of the surface density derived above. Because of the flaring nature of the gas layer, the mean midplane density decreases more rapidly with increasing R than does the surface density. The radial variation of the midplane density is shown in Fig. 10 for both the CO and for the H I data. The radial scalelength of 1.8 kpc derived for the CO/IRAS sources refers to the averaged northern and southern data at $R > 13$ kpc. The corresponding scalelength for the H I gas is 2.5 kpc. The average ratio of H I to H_2 midplane densities increases from 2.5 near the Sun to 80 near 19 kpc.

6. Conclusions

We have discussed the shape of the outer Galaxy as revealed by the distribution of molecular clouds with embedded IRAS sources and have compared this with the shape revealed by H I observations. The molecular-cloud distribution could be studied at larger distances than has previously been possible by identifying IRAS sources with appropriate colors as tracers of star forming regions. Of the 1302 selected IRAS sources, 1077 revealed CO $J = 1-0$ emission and subsequently provided a kinematic distance. Some of the conclusions listed below are summarized in Table 1.

1. We found CO emission at velocities as extreme as 110 km s^{-1}, corresponding to heliocentric distances of 15 kpc or galactocentric distances of 20 kpc. The absence of detected CO emission at more extreme velocities is not a consequence of the sensitivity of the IRAS survey or of the velocity range observed; evidently there are very few molecular clouds with embedded star formation at $R > 20$ kpc.

Table 1. Surface densities and thicknesses of the outer-Galaxy H I and H_2 distributions

R (kpc)	σ(H I) ($M_\odot$ pc^{-2})	σ(H_2) ($M_\odot$ pc^{-2})	$z_{1/2}$ (H I) (pc)	$z_{1/2}$ (H_2) (pc)
9	8.57	1.80	150	77
10	6.09	0.44	204	111
11	6.56	1.62	164	136
12	7.45	1.47	193	147
13	7.62	1.10	213	160
14	6.02	0.64	277	223
15	5.30	0.37	304	257
16	4.36	0.20	310	220
17	3.31	0.14	386	200
18	2.36	0.09	398	188
19	1.66	0.009	501	
20	1.23	0.015	582	
21	0.96	0.007	719	
22	0.80		810	
23	0.71		1018	
24	0.56		1163	

2. The longitude, velocity distribution of the outer-Galaxy CO clouds is similar to that of the H I, except that the H I emission can be traced to the more extreme velocities corresponding to $R = 24$ kpc.

3. The projected surface density of the molecular-cloud distribution shows some patchiness, but there is no dominant structure which extends from the second to the third quadrant.

4. The surface density distributions of IRAS sources at $R > 13$ kpc are approximately equal in the second and third quadrants. At $R < 13$ kpc the Perseus arm feature dominates the second quadrant distribution of both the IRAS sources and the H I.

5. The surface density of IRAS detections was converted to a measure of H_2 surface density. The ratio of H I to H_2 surface densities increases from a value of 5 near the Sun to 150 at $R = 19$ to 20 kpc.

6. The distribution of IRAS sources ends more abruptly at large R than that of H I. The mean radial scalelength describing the outer-Galaxy cutoff of the molecular cloud ensemble at $R > 13$ kpc is 1.5 kpc, whereas that of H I at $R > 13$ kpc is 4.0 kpc. The scalelength of the surface density of optically identified H II regions in the same region is 1.9 kpc.

7. The z-distribution of molecular clouds in the outer Galaxy shows the same warp as that of the H I gas layer.

8. The molecular clouds show the flaring of the outer Galaxy. The thickness of the galactic disk increases for $R > 10$ kpc at the same rate for the H I and CO tracers.

9. The scalelengths of the midplane densities are smaller than those of the surface densities because of the increase with R of the thickness of the galactic disk, as measured both for the diffuse H I layer and for the molecular cloud ensemble. The scalelength of the midplane densities at $R > 13$ kpc is 1.8 kpc for the IRAS-selected clouds and 2.5 kpc for the H I.

10. The mass of H_2 clouds in the outer Galaxy at $R > 8.5$ kpc is 5.8 10^8 $M_\odot$; the corresponding H I mass is 5.3 10^9 $M_\odot$.

Acknowledgements. Part of this work was done while JGAW was a guest at the Radioastronomisches Institut der Universität Bonn. We are grateful to the referee, L. Blitz, for his constructive comments on the manuscript.

References

Baldwin, J.E., Lynden-Bell, D., Sancisi, R.: 1960, *Monthly Notices Roy. Astron. Soc.* **193**, 313
Bloemen, J.B.G.M., Strong, A.W., Blitz, L., Cohen, R.S., Dame, T.M., Grabelsky, D.A., Hermsen, W., Lebrun, F., Mayer-Hasselwander, H.A., Thaddeus, P.: 1984, *Astron. Astrophys.* **154**, 25
Blitz, L., Fich, M., Stark, A.A.: 1982, *Astrophys. J. Suppl.* **49**, 183
Blitz, L., Fich, M., Kulkarni, S.: 1983, *Science* **220**, 1233
Bosma, A.: 1981, *Astron. J.* **86**, 1825
Brand, J.: 1986, Ph. D. Thesis, University of Leiden
Brand, J., Blitz, L., Wouterloot, J.G.A.: 1988, in *The Outer Galaxy*, eds. L. Blitz, F.J. Lockman, Springer, Berlin, Heidelberg, New York, p. 40
Brand, J., Blitz, L., Wouterloot, J.G.A., Kerr, F.J.: 1987, *Astron. Astrophys.* **68**, 1 (see also erratum *ibid.* **69**, 343)
Brinks, E., Burton, W.B.: 1984, *Astron. Astrophys.* **169**, 14
Bronfman, L., Cohen, R.S., Alvarez, H., May, J., Thaddeus, P.: 1988, *Astrophys. J.* **324**, 248
Burke, B.F.: 1957, *Astron. J.* **62**, 365
Burton, W.B.: 1976, *Ann. Rev. Astron. Astrophys.* **14**, 275
Burton, W.B.: 1985, *Astron. Astrophys. Suppl.* **62**, 365
Burton, W.B.: 1988a, in *The Outer Galaxy*, eds. L. Blitz, F.J. Lockman, Springer, Berlin, Heidelberg, New York, p. 94
Burton, W.B.: 1988b, in *Galactic and Extragalactic Radio Astronomy*, eds. G.L. Verschuur, K.I. Kellermann, Springer, Berlin, Heidelberg, New York, p. 295
Burton, W.B., Gordon, M.A.: 1978, *Astron. Astrophys.* **63**, 7
Burton, W.B., te Lintel Hekkert, P.: 1986, *Astron. Astrophys. Suppl.* **65**, 427
Clemens, D.P.: 1985, *Astrophys. J.* **295**, 422
Dame, T., Ungerechts, H., Cohen, R.S., de Geus, E., Grenier, I., May, J., Murphy, D.C., Nyman, L.-A., Thaddeus, P.: 1987, *Astrophys. J.* **322**, 706
Deul, E.R.: 1988, Ph. D. Thesis, University of Leiden
Fich, M., Blitz, L.: 1984, *Astrophys. J.* **279**, 125
Fich, M., Blitz, L., Stark, A.A.: 1989, *Astrophys. J.* **342**, 272
Grabelsky, D.A., Cohen, R.S., Bronfman, L., Thaddeus, P., May, J.: 1987, *Astrophys. J.* **315**, 122
Henderson, A.P., Jackson, P.D., Kerr, F.J.: 1982, *Astrophys. J.* **263**, 116
IRAS Point Source Catalog, Version 2: 1987, Government Printing Office, Washington
Jackson, P.D., FitzGerald, M.P., Moffat, A.F.J.: 1979, in *The Large-Scale Characteristics of the Galaxy*, ed. W.B. Burton, Reidel, Dordrecht, p. 221
Kerr, F.J.: 1957, *Astron. J.* **62**, 93
Kerr, F.J.: 1962, *Monthly Notices Roy. Astron. Soc.* **123**, 327
Kerr, F.J., Bowers, P.F., Jackson, P.D., Kerr, M.: 1986, *Astron. Astrophys. Suppl.* **66**, 373
Kerr, F.J., Lynden-Bell, D.: 1986, *Monthly Notices Roy. Astron. Soc.* **221**, 1023
Kimeswenger, S., Weinberger, R.: 1989, *Astron. Astrophys.* **209**, 51
Kulkarni, S.R., Blitz, L., Heiles, C.: 1982, *Astrophys. J.* **259**, L 63
Lockman, F.J.: 1984, *Astrophys. J.* **283**, 90
Maddalena, R.: 1986, Ph. D. Thesis, Columbia University
May, J., Alvarez, H., Garay, G., Murphy, D., Cohen, R.S.,

Thaddeus, P.: 1985, in *Proceedings of the ESO-IRAM-Onsala Workshop on (Sub)Millimeter Astronomy*, p. 245
May, J., Murphy, D.C., Thaddeus, P.: 1988, *Astron. Astrophys. Suppl.* **73**, 51
Mead, K.N.: 1988, in *The Outer Galaxy*, eds. L. Blitz, F.J. Lockman, Springer, Berlin, Heidelberg, New York, p. 201
Miyamoto, M., Yoshizawa, M., Suzuki, S.: 1988, *Astron. Astrophys.* **194**, 107
Oort, J.H., Kerr, F.J., Westerhout, G.: 1958, *Monthly Notices Roy. Astron. Soc.* **118**, 379
Rogstad, D.H., Wright, M.C.H., Lockhart, I.A.: 1976, *Astrophys. J.* **204**, 703
Sancisi, R.: 1983, in *Internal Kinematics and Dynamics of Galaxies*, ed. E. Athanassoula, Reidel, Dordrecht, p. 55
Sanders, D.B., Solomon, P.M., Scoville, N.Z.: 1984, *Astrophys. J.* **276**, 182
Shaver, P., McGee, R.X., Newton, L.M., Danks, A.C., Pottasch, S.R.: 1983, *Monthly Notices Roy. Astron. Soc.* **204**, 53
Weaver, H., Williams, D.R.W.: 1973, *Astron. Astrophys. Suppl.* **8**, 1
Wouterloot, J.G.A., Brand, J.: 1989, *Astron. Astrophys. Suppl.* **80**, 149 (Paper I)
Wouterloot, J.G.A., Brand, J., Henkel, C.: 1988a, *Astron. Astrophys.* **191**, 323
Wouterloot, J.G.A., Walmsley, C.M.: 1986, *Astron. Astrophys.* **168**, 237
Wouterloot, J.G.A., Walmsley, C.M., Henkel, C.: 1988b, *Astron. Astrophys.* **203**, 367